Facile fabrication of graphene@Fe-Ti binary oxide nanocomposite from ilmenite ore: An effective photocatalyst for dye degradation under visible light irradiation

Ngoc Tuan Truong[a,f], Hoai Phuong Nguyen Thi[a], Ha Duc Ninh[a], Xuan Thinh Phung[a], Chinh Van Tran[a], Thanh Tung Nguyen[b], Tien Dung Pham[c], Trung Dung Dang[d,*], Soon Woong Chang[f], Eldon R. Rene[g], Huu Hao Ngo[h], Dinh Duc Nguyen[e,*], Duong Duc La[a,]**

[a] *Institute of Chemistry and Materials, Nghia Do, Cau Giay, Ha Noi, Vietnam*
[b] *Institute of Materials Science, Vietnam Academy of Science and Technology, Cau Giay, Ha Noi, Vietnam*
[c] *Environmental Institute, Viet Nam Maritime University, 484 Lạch Tray, Dong Quoc Binh, Le Chan, Hai Phong, Vietnam*
[d] *School of Chemical Engineering, Hanoi University of Science and Technology, Hai Ba Trung, Ha Noi, Vietnam*
[e] *Institute of Research and Development, Duy Tan University, Da Nang 550000, Vietnam*
[f] *Department of Environmental Energy Engineering, Kyonggi University, 154-42, Gwanggyosan-ro, Yeongtong-gu, Suwon-si, Gyeonggi-do, Republic of Korea*
[g] *Department of Water Supply, Sanitation and Environmental Engineering, IHE Delft Institute for Water Education, Westvest 7, 2611AX, Delft, the Netherlands*
[h] *Centre for Technology in Water and Wastewater, School of Civil and Environmental Engineering, University of Technology Sydney, Sydney, NSW, 2007, Australia*

Keywords: Graphene nanoplates; graphene@Fe-Ti binary oxide composite; Adsorption; Ilmenite ore; Dye degradation; Photocatalysis

Abstract

Photocatalysis is an effective treatment technique for the removal of toxic pollutants present in water and wastewater. In this study, graphene@Fe-Ti binary oxide composites was prepared using a hydrothermal method and characterized by scanning electron microscopy, transmission electron microscopy, X-ray diffraction, Fourier- transform infrared spectroscopy, and Brunauer-Emmett-Teller surface area analysis. The prepared composite exhibited even distribution of the Fe-Ti binary oxide on the surface of graphene, with an average diameter of
16.4 nm and a surface area of 133.7 m^2/g. The optical property was evaluated and the band gap was calculated to be 2.867 eV using solid-state UV–vis spectroscopy and the $[F(R)hv]^{1/2}$ plot. Lab-scale experiments were performed to evaluate the performance of graphene@Fe-Ti binary oxides to remove methyl blue (i.e. a dye) from wastewater. It was observed that the graphene loading had a significant effect on the photocatalytic activity of the composite and a composite with 20 % graphene showed the highest photocatalytic activity, with 100 % removal of the dye, after 20 min of irradiation time and a degradation rate constant of 0.213 min^{-1}. Besides, the possible photocatalytic dye degradation mechanism using graphene@Fe-Ti binary oxide composite has also been proposed.

1. Introduction

Methylene blue (MB) dye is commonly present in wastewater discharged from the textile industry. The presence of MB dye in water bodies/natural environment can affect the water quality, soil property, agricultural productivity and also damage the flora and fauna in the environment [1,2]. Photocatalysis using heterogeneous materials is a rapidly growing field of applied research for the degradation of toxic organic compounds from aqueous solutions [3–6]. Using incident light irradiation, the heterogeneous photocatalysts generate highly reactive and oxidizing hydroxyl radicals, which could degrade toxic organic compounds to non-hazardous/innocuous compounds [7–9]. Many semiconductor oxides such as ZnO, CuO, TiO_2, CaS, ZnS, and MoS_2 have been studied and tested as photocatalysts for addressing environmental issues associated with aqueous media. Among them, TiO_2 has attracted the most attention from researchers for photocatalysis, owing to its high photocatalytic activity [10–15]. However, as TiO_2 has poor light-absorption capability in the range of visible wavelength, many research studies have been dedicated to combine TiO_2 with other materials that could enable the photocatalytic activity under the visible spectrum of

* Corresponding author.
** Corresponding author.
E-mail addresses: dung.dangtrung@hust.edu.vn (T.D. Dang), nguyendinhduc2@duytan.edu.vn, nguyensyduc@gmail.com (D.D. Nguyen), duc.duong.la@gmail.com (D.D. La).

sunlight energy [16–18].

Hybrids of many metal oxides, including WO_3, MoO_3, SiO_2, Fe_3O_4 and ZrO_2, with TiO_2 have been prepared to improve the light absorption capacity and photocatalytic activity of the catalysts [19–24]. Iron oxide (Fe_2O_3) is an n-type semiconductor, which is commonly used as a photocatalyst in water splitting and the degradation of organic compounds because it is inexpensive, abundant, non-toxic, and remains stable during photocatalytic reactions [25–30]. The bandgap of Fe_2O_3 is smaller (2.3 eV) than that of TiO_2 (3.2 eV), which is suitable for absorbing light in the visible region; however, its low conductivity and a short excited diffusion length (2−20 nm) significantly reduces its photocatalytic activity [31,32]. The combination of TiO_2 and Fe_2O_3 have been extensively studied to improve the absorption efficiency in the visible region and to increase the photocatalytic activity through the synergetic effect of the two metals [33–38].

It is well-known that the main source of raw material for TiO_2 is ilmenite ore ($FeTiO_3$) [39,40]. Previous works have also used ilmenite ore as a raw material to fabricate Fe_2O_3/TiO_2 composites [41]. For example, ilmenite ore was treated with sulfuric acid to synthesize a Fe_2O_3-TiO_2 composite [42] that showed high photocatalytic activity during the oxidation of 4-chlorophenol in water under light irradiation. In another study, Fe_2O_3-TiO_2 composite was used as a catalyst for the conversion of vegetable oil to biodiesel [43]. Since its discovery in 2004, graphene, one of the carbon materials with a two-dimensional (2D) structure, has attracted much attention from scientists [44–47]. Graphene has exceptional mechanical, chemical, and physical properties, and it can be employed in many applications such as in biosensors, composites, smart textiles, energy storage devices, and for solar energy harvesting and conversion [48–51]. Most recently, owing to its large surface area, superior mechanical flexibility, and especially high electron conductivity and mobility, graphene has been utilized as a supporting material for enhancing the efficiency of photocatalytic reactions [52–56]. It could be used as a support and promoter to enhance charge separation [57,58], surface area [59] and it also plays an important role in enhancing the adsorption efficiency [58,60,61].

Zhang *et al*. [62] employed a combustion based approach to successfully fabricate a visible-light responsive magnetic Fe_2O_3/TiO_2/graphene composite using metals salts and graphene oxide as precursors [62]. The resultant photocatalyst absorbs light over a wider visible-light range and show improvised visible-light photocatalytic performance owing to reduced charge recombination. In this study, a simple approach to fabricate graphene@Fe-Ti binary oxide composites using a cheap and abundant source of ilmenite ore and graphene has been proposed. The chemical and physical properties of the materials were characterized and the photocatalytic performance of the composite was tested for the degradation of a dye, methyl blue (MB). The effect of graphene loading on the photocatalytic efficiency was studied, and finally, the photocatalytic mechanism of dye removal has been proposed.

2. Materials and methods

2.1. Chemicals

Ilmenite ore (52 %) was obtained from Cat Khanh Mine, Binh Dinh Province, Vietnam. Ethanol (C_2H_5OH, 96 %) was purchased from Duc Giang Chemicals and Detergent Powder Co., Ltd. Acetone (99 %), H_2SO_4 (98 %), $KHSO_4$ (> 95 %), $K_2S_2O_8$ (99 %), and graphite flakes (< 180 μm, > 90 %) were obtained from Xilong Scientific Co., Ltd. Analytical grade methylene blue (99 %) was purchased from Sigma-Aldrich Pvt. Ltd. Distilled water was used for the preparation of all the solutions. All chemicals were used as received without any further purification.

2.2. Preparation of a Fe-Ti salt solution from ilmenite ore (solution A)

Ilmenite ore (52 %, $FeTiO_3$) was washed thoroughly with distilled water, dried in a heating oven, and milled in a ball milling machine until the particle size was < 0.149 mm (passed through a 100-mesh sieve). Thereafter, 5 g of the milled ilmenite ore was mixed with 35 g of $KHSO_4$ and the mixture was calcined at 600 °C for 2 h. After the calcination, the slag was leached in a 10 % H_2SO_4 solution. After the removal of residues, a solution containing the leached metal ions was obtained.

2.3. Preparation of graphene nanoplates (GNPs)

Graphene was synthesized by a facile one spot method, as described elsewhere [63]. Natural graphite flakes were washed several times with distilled water and 2 g of the washed flakes was dispersed in concentrated sulfuric acid (98 %). The mixture was stirred using a magnetic stirrer and then 10 g of $K_2S_2O_8$ was added. The reaction mixture was stirred continuously for 3 h. After that, the residue was filtered, washed several times with acetone, and dried at 90 °C in a heating oven.

2.4. Preparation of graphene@Fe_2O_3/TiO_2 nanocomposites

A mixture of 50 mL of ethanol and 100 mL of solution A was stirred for 30 min to form a homogeneous solution (solution B). A known amount of graphene (0, 10, 20, or 40 mg, labelled as TCG0, TCG10, TCG20, and TCG40, respectively) was added to solution B and then the mixture was ultra-sonicated for 30 min to uniformly disperse the graphene in the solution. After that, the mixture was transferred to an autoclave to carry out the hydrothermal reaction at 150 °C for 8 h. The precipitate obtained was vacuum filtered and washed several times with distilled water until SO_4^{2-} ions were completely removed and the pH of the solution became neutral. Thereafter, the residue was dried at 80 °C in a heating oven.

2.5. Characterization of the synthesized composites

The morphology of the material was characterized by scanning electron microscopy (SEM; Hitachi S-4600) and transmission electron microscopy (TEM; EMLab NIHE). The distance between the graphene layers was determined by high-resolution transmission electron microscopy (HRTEM; 200 kV with field emission, TECNAI G2-20 S-TWIN, FEI). The crystalline structure of the synthesized materials was characterized by X-ray diffraction (XRD) with the X'Pert Pro instrument using Cu $K\alpha$ radiation. An X-ray source voltage of 45 kV and electron beam current of 40 mA were used and the patterns were recorded over the scanning angle 2θ ranging from 5 to 90° in steps of 0.5°. The Fourier-transform infrared (FT-IR) spectra of the samples were recorded on a Bruker spectrometer in a range of 4000 to 600 cm^{-1}. Ultraviolet-visible diffuse reflectance spectroscopy (UV–vis DRS) was performed in the range of 200–2500 nm using a $BaSO_4$ plate as the reflectance standard.

2.6. Photocatalytic activity test

The photocatalytic activities of the samples were evaluated based on the degradation of MB in an aqueous solution under a 350 W xenon sunlight simulated lamp (AHD 350, Shenzhen Anhongda Opto Technology Co. Ltd., China) in a reaction chamber. Aliquots (5 mL) of the aqueous solution of MB (10 mg/L, pH = 7.0) were placed in several 6 mL quartz tubes, and 6 mg of the synthesized graphene@Fe_2O_3/TiO_2 nanocomposite was added into each tube. The tubes were placed on a flat mirror plate and a certain distance was maintained between the mirror plate and the lamp. Before light irradiation, the aqueous suspensions were magnetically stirred in the dark for 1 h to achieve the adsorption-desorption equilibrium. The reaction chamber was

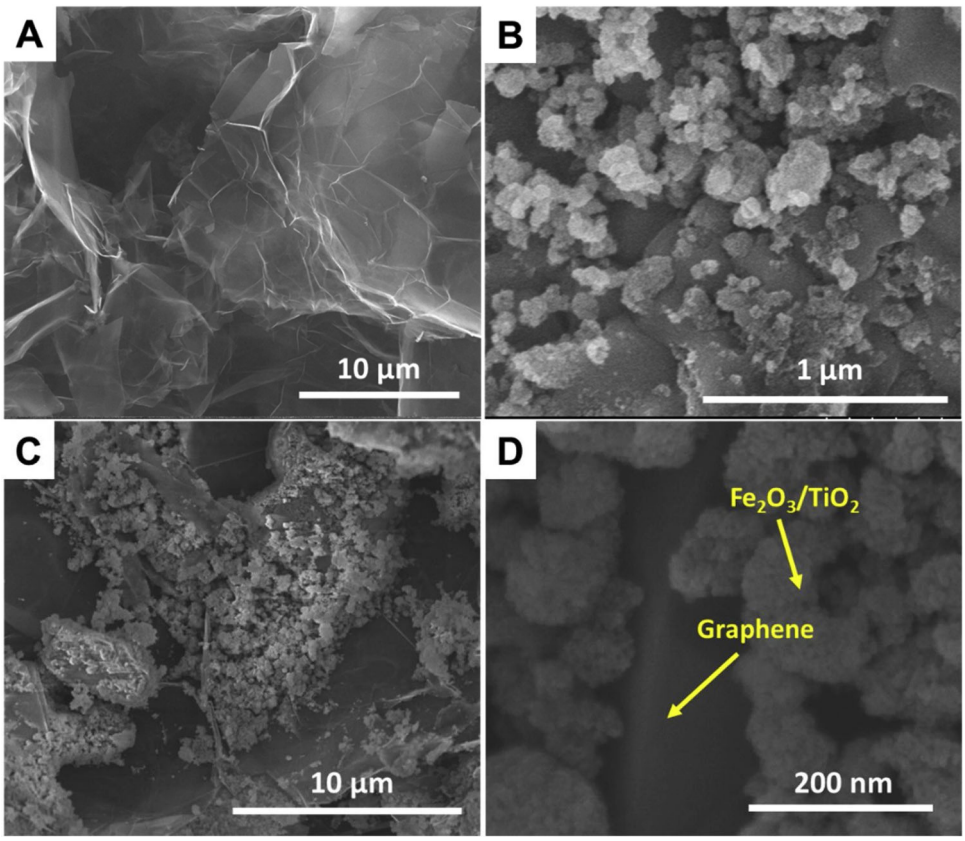

Fig. 1. SEM images of the graphene nanoplates (A), free-standing Fe-Ti binary oxide (B), and graphene@Fe-Ti binary oxide (C and D).

mechanically ventilated to maintain a constant temperature (~35 °C) during illumination. After every 5-min time interval, one quartz tube was taken out and the liquor was extracted by centrifugation to remove the solid. The absorption at 668 nm was determined to evaluate the photocatalytic performance of the composite using a Cary 5000 UV–vis-NIR spectrophotometer. The photocatalytic tests were carried out under similar conditions in the presence of different photocatalysts (TCG0, TCG10, TCG20, TCG40, and GNPs).

3. Results and discussion

3.1. Morphological characteristics of the graphene@Fe-Ti binary oxide nanocomposite

Graphene nanoplates (GNPs) were fabricated by adopting the approach from a previous work, wherein natural graphite was chemically exfoliated with an oxidant and highly concentrated sulfuric acid to form GNPs. The obtained GNPs has a bulk density of 0.015 g/cm^3 and a carbon content of 99.6 % [63]. The surface morphology of the GNPs was observed by SEM (Fig. 1A). It is obvious that GNPs have wrinkled and crumpled morphology with 10−30 µm lateral diameter and less than 20 nm thickness. As illustrated in Figs. 1B and S1, the morphology of the Fe-Ti binary oxide prepared from ilmenite according to a similar process without the addition of the GNPs, clearly indicates that the prepared Fe-Ti binary oxide is in the form of nanoparticles with size distribution in the range of 50–150 nm.

The surface morphology of the GNPs@Fe-Ti binary oxide composites are shown in Fig. 1C and D. At low resolution (Fig. 1C), the good distribution of the Fe-Ti binary oxide particles on the graphene surface can be clearly observed. The high-magnification SEM image of the composite (Fig. 1D) reveals a much smaller particle size of the Fe-Ti binary oxide (less than 20 nm) formed on the GNP surface compared to that of free-standing Fe-Ti binary oxide prepared from ilmenite ore without the assistance of graphene. This is probably due to the presence of graphene, which assists the nucleation of Fe-Ti binary oxide evenly on its surface and their uniform growth with control over the particle size, leading to small Fe-Ti binary oxide particles.

The surface structure of the GNPs@Fe-Ti binary oxide composites was further investigated by TEM and HRTEM studies. Figs. 2A and S2 shows the low-magnification TEM image of the composite, which clearly indicates that the Fe-Ti binary oxides are uniform with an average particle size of ~ 13.6 nm, which is in good agreement with the SEM results. The inset of Fig. 2A shows the high-resolution HRTEM image of the composite, which shows the edges of graphene with multilayers bonding to the Fe-Ti binary oxide particles. The HRTEM image of Fe-Ti oxide (Fig. 2B) shows lattice fringe spacing of both TiO_2 and Fe_2O_3, which can be attributed to the formation of heterojunctions between Fe_2O_3 and TiO_2 [64]. This close contact can contribute to the improvement in the charge transfer as the length of the carrier diffusion is short, and as a result, the charge recombination is suppressed, which is essential for the enhancement of the photocatalytic activity. The inset of Fig. 2B shows the selected-area electron diffraction (SAED) pattern of the Fe-Ti binary oxide, which exhibits polycrystalline rings of TiO_2 and Fe_2O_3 phases.

The nature of chemical bonding was investigated by FTIR spectroscopy. The FTIR spectra of graphene, free-standing Fe-Ti binary oxides, and graphene@Fe-Ti oxides are shown in Fig. 3A. In the FTIR spectrum of graphene (black line), there are no obvious stretching peaks, which is a strong indication of the presence of pristine graphene sheets without defects. The defects gave rise to peaks at 3400 cm^{-1} (OH), 1720 cm^{-1} (CO), 1600 cm^{-1} (skeletal vibrations from unoxidized graphitic domains), 1220 cm^{-1} (COH), and 1060 cm^{-1} (CO), respectively, which are the characteristic peaks of graphite and graphene oxides. Both the spectra of the free-standing binary oxide (red line) and graphene@Fe_2O_3/TiO_2 composite (blue line) have a broad absorption band at 3200 cm^{-1} and a sharp one at 1631 cm^{-1} corresponding to the

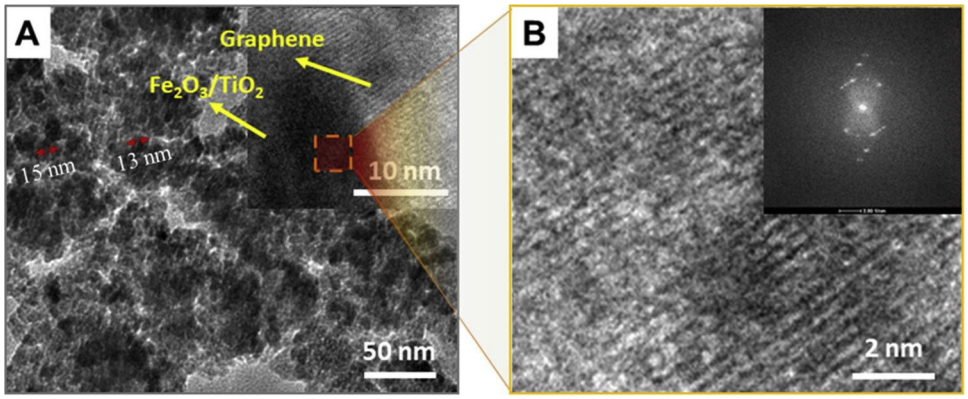

Fig. 2. HRTEM image (A) and SAED pattern (B) of graphene@Fe-Ti binary oxide composite.

stretching and bending vibrations of OeH, respectively. In the FTIR spectrum of free-standing Fe-Ti binary oxide, the bands at 998 and 443 cm^{-1} are related to the TieOTi and FeOee vibrations of TiO_2 and Fe_2O_3crystalline phases, respectively. Interestingly, when combined with graphene, a shift in the TieOTei vibration was observed, indicating good interaction between the FeeTi binary oxide and graphene.

The crystallinity of the graphene@Fe-Ti binary oxide composites was studied by XRD (Fig. 3B). The XRD pattern of the as-prepared composite shows high-intensity peaks at 2θ = 25.7, 38.2, 48.3, 54.2, 63, and 69.1°, corresponding to the characteristic pattern of the anatase phase with miller indices of 101, 004, 200, 211, 204, and 220, respectively (JCPDS card number 21–1272). There are no peaks of the rutile phase, which demonstrates the formation of high-purity anatase phase, which is mainly responsible for the enhanced photocatalytic activity of TiO_2. The characteristic peak of graphene in the XRD pattern is not obvious, which might be due to the overlap of the strong peaks of TiO_2 anatase and the natural graphene. The broad nature of the peaks implies that the Fe-Ti binary oxide particles are relatively small in size. The peaks intensity of the Fe_2O_3 is negligible, which is probably due to the low crystallinity of the Fe_2O_3 in comparison to the TiO_2 in the Fe-Ti binary oxide particles. Since the particle size of this binary oxide as observed in the SEM and TEM images is < 100 nm, the average size of the mixed oxides can be calculated using the Debye-Scherrer equation. The average crystal size of Fe-Ti binary oxide on the GNP surface was calculated to be 16.4 nm, which is in good agreement with the TEM results. The weight percentages of C, O, Ti and Fe elements in graphene@Fe-Ti binary oxides were found to be 12.08, 64, 10.89, and 3.6 %, respectively (Fig. S3). The remaining weight percentage can be ascribed to the impurities from the primary ores and oxidants during the fabricating process.

The thermal property of the graphene@Fe-Ti binary oxides with 30 % graphene loading was investigated by the thermal gravimetric analysis (TGA), as shown in Fig. S4. The TGA curve shows a negligible decrease in weight loss at 200 °C indicating low content of free water on the surface of the material. From 200 °C to 600 °C, a weight loss of ~ 10 % was ascribed to the dehydration of water-chemisorbed to the metal oxide. The significant weight loss of the composite after 600 °C is due to the burning of graphene, i.e. due to its reaction with oxygen.

The total surface area of the graphene@Fe-Ti binary oxide composite was calculated using the N_2 adsorption/desorption isotherm (Fig. S5). The calculated Brunauer-Emmett-Teller (BET) surface area of the Fe-Ti binary oxide and the graphene@Fe-Ti binary oxide were 58 and 133.7 m^2/g, respectively. This clearly indicates that the addition of graphene significantly improves the surface area of Fe-Ti binary oxide, which in turn, improves its photocatalytic performance. The pore volume and pore size of the graphene@Fe-Ti binary oxide composite were 0.01 cm^3/g and < 20.65 nm, respectively, which are reasonable for photocatalytic application. The optical properties of the graphene@Fe-Ti binary oxide composite were investigated by solid-state UV–vis diffuse reflectance spectroscopy (Fig. 4A). The UV–vis spectrum of the synthesized composite has three absorbance peaks at a λ_{max} of ~420,

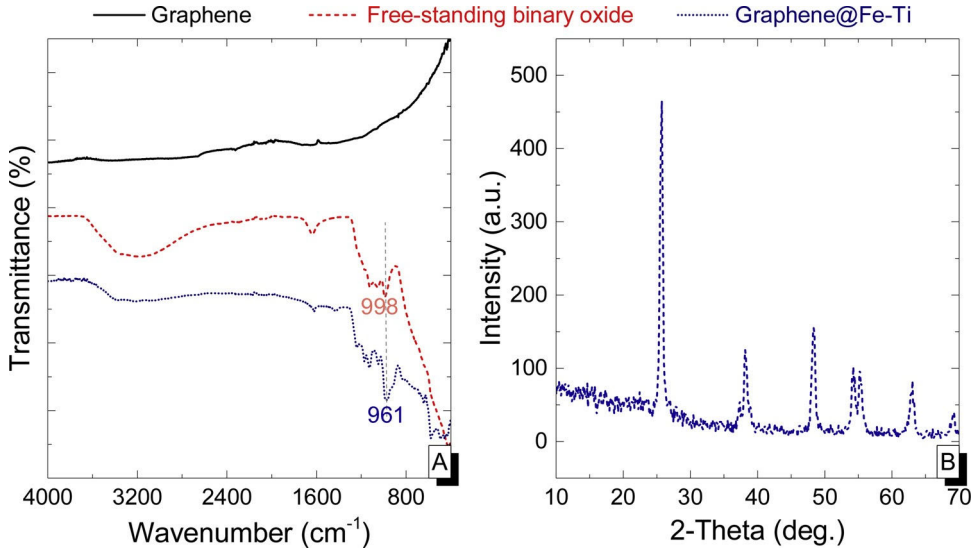

Fig. 3. FTIR spectra (A) and XRD pattern (B) of graphene@Fe-Ti binary oxide composite.

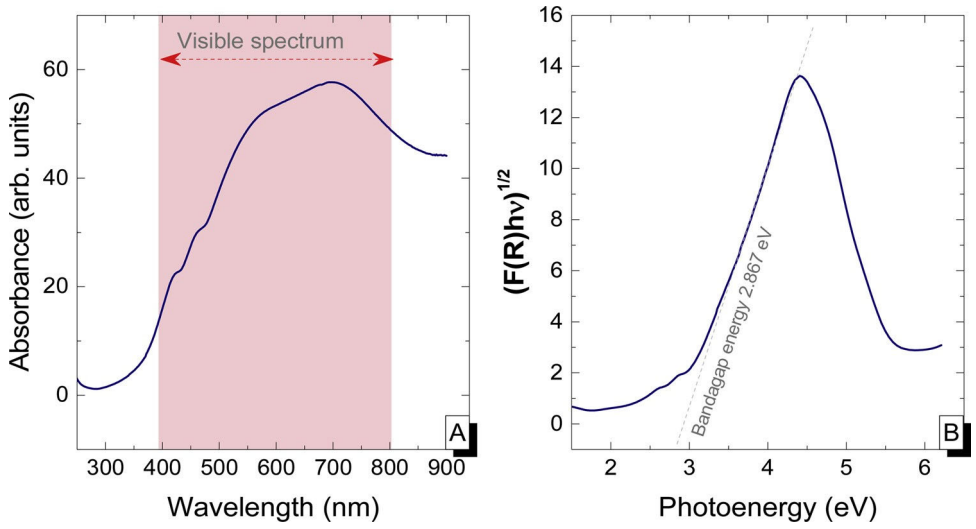

Fig. 4. Solid-state UV–vis spectrum (A) and $[F(R)h\nu]^{1/2}$ plot (B) to determine the bandgap of the graphene@Fe-Ti binary oxide composite.

550, and 690 nm, ascribed to the presence of Fe ions in the material, which shifts the optical absorption edge from UV to the visible light range (i.e., a red shift). Figs. 4B and S6 displays the $[F(R)h\nu]^{1/2}$ plot for indirect transition according to the Kubelka-Munk function, F(R), which is equivalent to the absorbance of the material in the UV–vis spectrum; $h\nu$ is the photon energy, $h\nu = (1239/\lambda)$ eV, where λ is the wavelength in nm. The value of $h\nu$ is extrapolated to $F(R)h\nu = 0$, which gives the absorption energy corresponding to the band gap E_v. It could be observed that the E_v of Fe-Ti binary oxide and graphene@Fe-Ti binary oxide composite is smaller than that of pristine TiO_2 (~ 3.2 eV). The bandgap of Fe-Ti binary oxide and graphene@Fe-Ti binary oxide composite were 2.73 and 2.867 eV, respectively; thus, the composite could have photocatalytic activity in the range of visible light.

3.2. Degradation of methylene blue using graphene@Fe-Ti binary oxide nanocomposite and proposed mechanism

Since the bandgap of the prepared graphene@Fe-Ti binary oxide is > 2.867 eV, it could also have photocatalytic activity in the visible light region. Thus, the photocatalytic degradation of MB dye using graphene@Fe-Ti binary oxide (TCG10, TCG20, and TCG40), fabricated with various graphene contents, and free-standing Fe-Ti binary oxide (TCG0) were evaluated. The change in the absorption peak at 668 nm of MB as a function of time was monitored to assess the photocatalytic performance. Fig. 5A reveals the MB removal (%) versus time under various experimental conditions of the photocatalytic reaction. It is obvious that, when no photocatalyst was used, there was negligible degradation of MB, which indicates that no self-sensitized photodegradation of MB occured. Similarly, when graphene nanoplates (GNPs) were employed as a photocatalyst, an insignificant decrease in the concentration of MB was observed.

However, when Fe-Ti binary oxide photocatalyst was used, the concentration of MB decreased by ~60 % after only 20 min under simulated sunlight irradiation. This result demonstrates that the Fe-Ti binary oxide has good photocatalytic activity toward MB dye in the visible-light region. The MB removal efficiency varied according to the graphene content; the composite with a graphene content of 20 % showed the highest photocatalytic activity toward MB with a 100 % removal after 20 min of irradiation time under simulated sunlight. This is probably due to the high conductivity of graphene, which contributes to the separation of the electron-hole pairs generated by the Fe-Ti binary oxide semiconductor, owing to which more electrons and holes become available for MB degradation. The plot of $\ln(C_t/C_0)$ *vs.* time (Fig. 5B) was used to infer the kinetics of the photocatalytic reaction of MB in the presence of photocatalysts, where C_t is the peak intensity at time t, and C_o is the intensity at time zero. From these plots, the degradation rate constant of MB by the graphene@Fe-Ti binary oxide photocatalyst containing 20 % graphene was determined to be 0.213 min^{-1}.

The effect of initial MB dye concentration on the photodegradation performance of graphene@Fe-Ti binary oxide was studied at a catalyst concentration of 1 g/L, with various MB concentrations ranging from 10 to 100 mg/L (Fig. S7). It can be seen from the figure that the higher MB removal was observed at the lower MB concentration. After 30 min of irradiation time under simulated sunlight, the removal of MB from water was 100, 91.2, 73.3, 67.4, 56.9, and 45.8 % at an initial MB concentration of 10, 20, 40, 60, 80, and 100 mg/L, respectively. The stability and reusability of the graphene@Fe-Ti binary oxide was evaluated by repeatedly carrying out the MB photodegradation tests over graphene@Fe-Ti binary oxide under visible-light irradiation. After the first cycle of MB degradation tests, the graphene@Fe-Ti binary oxide was separated from the reaction system and dried at 80 °C for 6 h. The photocatalyst was reused for the next subsequent cycles and the results are shown in Fig. 6. It can be seen that the decrease in the MB degradation efficiency is less than 10 % after 4 cycles of reuse, which indicates that the activity of graphene@Fe-Ti binary oxide as a photocatalyst is relatively stable and it can be reused several more times with reasonable removal performance. Thus, the graphene@Fe-Ti binary oxide photocatalyst is a promising material for wastewater remediation because of its excellent photocatalytic activity, cost-effectiveness and recyclability.

Besides, the COD of methyl blue was measured before and after photocatalytic treatment with graphene@Fe-Ti binary oxide. The initial and final COD values were 182.4 and 10.2 mg/L, respectively, resulting in ~ 95 % removal. This result is also consistent with several previous results, wherein authors have reported the degradation of MB dyes into carbon dioxide and water. During the degradation process, graphene could be used as a support and promoter to improve charge separation by suppressing the recombination of electron-hole pairs generated by the irradiation of Fe-Ti binary oxide, thereby increasing the lifetime of the charge carriers, as a result, enhancing the photocatalytic activity [58]. Thus, graphene also plays an important role in enhancing the efficiency of dye adsorption, as it facilitates interfacial charge transfer interaction with the adsorbed agent [58]. In order to investigate the enhanced photo-generated charge carrier transfer, electron-hole separation, and migration in the photocatalysts due to the addition of graphene, the photoluminescence (PL) spectra was obtained (Fig. S8). When the PL intensity is low, the electrons and holes actively

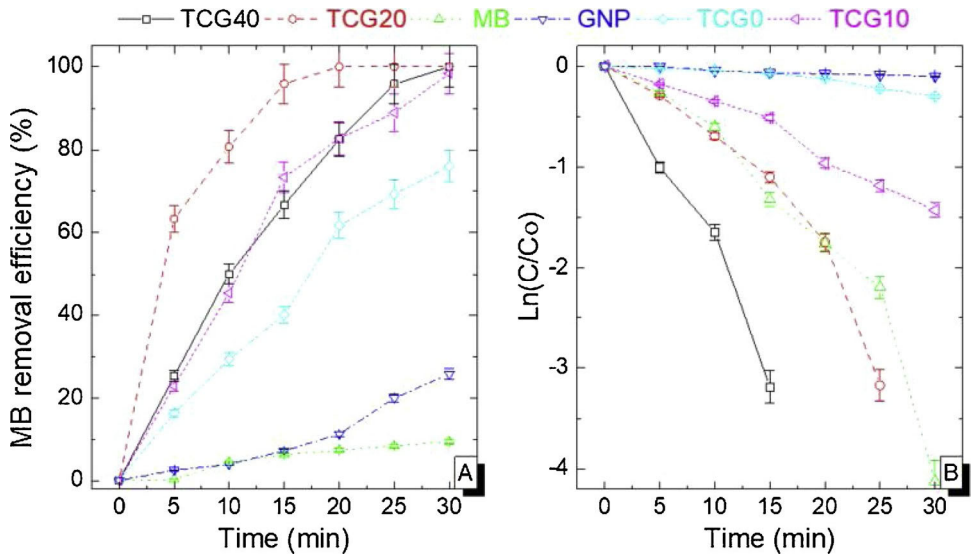

Fig. 5. (A) Photocatalytic performance and (B) kinetic simulation curve for methyl blue degradation without catalyst (black line), GNPs (red line), free-standing Fe-Ti binary oxide (green line), and graphene@Fe-Ti binary oxide, at different graphene loadings.

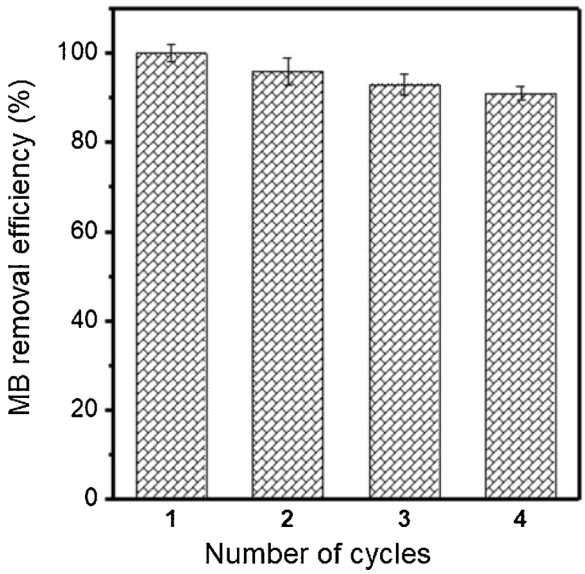

Fig. 6. Stability and recyclability of the graphene@Fe-Ti binary oxide.

participate in the redox reactions to generate active species such as peroxides and OH- radicals for the degradation of pollutants. Fig. S8 shows the PL spectra of the Fe-Ti binary oxide and graphene@Fe-Ti binary oxide excited at 335 nm. It can be clearly seen that the presence of graphene significantly increases the electrons/holes separation as the PL spectrum of the graphene@Fe-Ti binary oxide is much lower than that of Fe-Ti binary oxide. Therefore, the introduction of graphene significantly enhances the photocatalytic performance of the photocatalysts semiconductor property.

Besides, the COD of methyl blue was measured before and after photocatalytic treatment with graphene@Fe-Ti binary oxide. The initial and final COD values were 182.4 and 10.2 mg/L, respectively, resulting in ~ 95 % removal. This result is also consistent with several previous results, wherein authors have reported the degradation of MB dyes into carbon dioxide and water. During the degradation process, graphene could be used as a support and promoter to improve charge separation by suppressing the recombination of electron-hole pairs generated by the irradiation of Fe-Ti binary oxide, thereby increasing the lifetime of the charge carriers, as a result, enhancing the photocatalytic activity [58]. Thus, graphene also plays an important role in enhancing the efficiency of dye adsorption, as it facilitates interfacial charge transfer interaction with the adsorbed agent [58]. In order to investigate the enhanced photo-generated charge carrier transfer, electron-hole separation, and migration in the photocatalysts due to the addition of graphene, the photoluminescence (PL) spectra was obtained (Fig. S8). When the PL intensity is low, the electrons and holes actively participate in the redox reactions to generate active species such as peroxides and OH- radicals for the degradation of pollutants. Fig. S8 shows the PL spectra of the Fe-Ti binary oxide and graphene@Fe-Ti binary oxide excited at 335 nm. It can be clearly seen that the presence of graphene significantly increases the electrons/holes separation as the PL spectrum of the graphene@Fe-Ti binary oxide is much lower than that of Fe-Ti binary oxide. Therefore, the introduction of graphene significantly enhances the photocatalytic performance of the photocatalysts semiconductor property.

Based on the above results and scientific discussion, a possible mechanism for dye degradation using graphene@Fe-Ti binary oxide composite under visible-light irradiation has been proposed (Fig. 7). Under the irradiation of visible light, the composite generates electron-hole pairs and the electrons are transferred from the valence band (VB) to the conduction band (CB) of the Fe-Ti oxide semiconductor [65]. The generated electrons then move to the graphene sheets and enhances the charge separation; as a result, the recombination of electrons and holes is prevented. The photo-generated holes would react with H_2O or OH^-

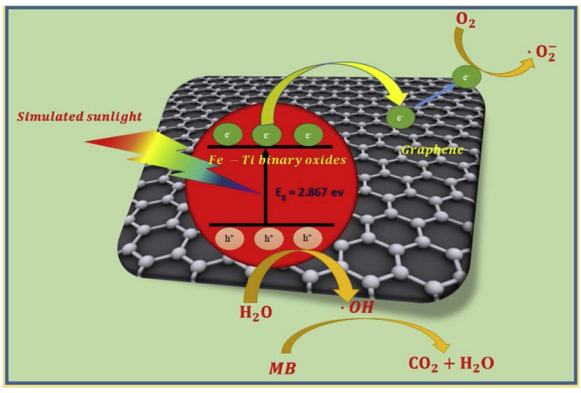

Fig. 7. Proposed photocatalytic mechanism of MB degradation catalyzed by graphene@Fe-Ti binary oxide.

to form active species such as ·OH, which participate in the oxidation process of dye molecules to form degraded products on the surface of the Fe-Ti binary oxide [66]. Further, the generated electrons reduce the O_2 dissolved in water to form $O_2^{\bullet-}$ radicals on the surface of graphene [67].

4. Conclusions

In this study, graphene@Fe-Ti binary oxide composite (size: 16.4 nm; surface area of 133.7 $m^2\ g^{-1}$) was fabricated using a one-pot hydrothermal method from ilmenite ore. The results from optical study reveals that the composite has a lower bandgap (2.867 eV) than that of pristine anatase (3.2 eV), which enables the composite to have photocatalytic activity in the visible-light region. The graphene@Fe-Ti binary oxide exhibited high photocatalytic performance for the degradation of MB dye, i.e. 100 % removal, in ~ 20 min of irradiation with simulated sunlight. The degradation rate constant of MB in the presence of graphene@Fe-Ti binary oxide photocatalyst was 0.213 min^{-1}. With high photocatalytic performance, a simple method of fabrication using ilmenite, easy recoverability and reusability, the graphene@Ti-Fe binary oxide composite offers significant environmental applications in the future.

Declaration of Competing Interest

The authors declare that they have no known competing financial interests or personal relationships that could have appeared to influence the work reported in this paper.

Acknowledgements

This research was funded by the Vietnam National Foundation for Science and Technology Development (NAFOSTED) fund, under the grant agreement number 104.05-2019.01. ERR thanks IHE Delft Institute for Water Education for providing infrastructural and staff time support (Project: Support to Society) to collaborate with researchers from South Korea, Vietnam and Australia.

Appendix A. Supplementary data

Supplementary material related to this article can be found, in the online version, at doi:https://doi.org/10.1016/j.jwpe.2020.101474.

References

[1] M. Iqbal, *Vicia faba* bioassay for environmental toxicity monitoring: a review, Chemosphere 144 (2016) 785–802.
[2] A. Shindy, Problems and solutions in colors, dyes and pigments chemistry: a review, Chem. Int. 3 (2) (2017) 97–105.
[3] I. Thakur, B. Örmeci, A. verma, Inactivation of *E. coli* in water employing Fe-TiO_2 composite incorporating in-situ dual process of photocatalysis and photo-Fenton in fixed-mode, J. Water Proc. Eng. 33 (2020) 101085.
[4] C.P.Md Oliveira, M.M. Viana, M.C.S. Amaral, Coupling photocatalytic degradation using a green TiO_2 catalyst to membrane bioreactor for petroleum refinery wastewater reclamation, J. Water Proc. Eng. (2019) 101093.
[5] A. Akhundi, A. Habibi-Yangjeh, M. Abitorabi, S. Rahim Pouran, Review on photocatalytic conversion of carbon dioxide to value-added compounds and renewable fuels by graphitic carbon nitride-based photocatalysts, Catal. Rev. 61 (4) (2019) 595–628.
[6] M. Pirhashemi, A. Habibi-Yangjeh, S.R. Pouran, Review on the criteria anticipated for the fabrication of highly efficient ZnO-based visible-light-driven photocatalysts, J. Ind. Eng. Chem. 62 (2018) 1–25.
[7] R. Andreozzi, V. Caprio, A. Insola, R. Marotta, Advanced oxidation processes (AOP) for water purification and recovery, Catal. Today 53 (1) (1999) 51–59.
[8] R. Shanmuganathan, F. Lewis Oscar, S. Shanmugam, N. Thajuddin, S.A. Alharbi, N.S. Alharbi, et al., Core/shell nanoparticles: synthesis, investigation of antimicrobial potential and photocatalytic degradation of Rhodamine B, J. Photochem. Photobiol. B: Biol. 202 (2020) 111729.
[9] J. Lin, H. Hu, N. Gao, J. Ye, Y. Chen, H. Ou, Fabrication of GO@MIL-101(Fe) for enhanced visible-light photocatalysis degradation of organophosphorus contaminant, J. Water Proc. Eng. 33 (2020) 101010.
[10] M.R. Hoffmann, S.T. Martin, W. Choi, D.W. Bahnemann, Environmental applications of semiconductor photocatalysis, Chem. Rev. 95 (1) (1995) 69–96.
[11] A.K. Adepu, S. Siliveri, S. Chirra, S. Goskula, S.R. Gujjula, R. Anumula, et al., A novel porous Fe_3O_4/Titanosilicate/g-C_3N_4 ternary nanocomposites: synthesis, characterization and their enhanced photocatalytic activity on Rhodamine B degradation under sunlight irradiation, J. Water Proc. Eng. 34 (2020) 101141.
[12] S. Guan, M. Al Amin Bin Fadhli, L. Hao, H. Yoshida, Y. Cheng, K. Zhou, et al., Fabrication and characterization of environmental purification unit using photocatalytic balls with heterojunction, J. Water Proc. Eng 31 (2019) 100858.
[13] R. Geng, J. Yin, J. Zhou, T. Jiao, Y. Feng, L. Zhang, et al., In situ construction of Ag/TiO_2/g-C_3N_4 heterojunction nanocomposite based on hierarchical co-assembly with sustainable hydrogen evolution, Nanomaterials 10 (1) (2020) 1.
[14] Y. Feng, J. Yin, S. Liu, Y. Wang, B. Li, T. Jiao, Facile Synthesis of Ag/Pd nanoparticle-loaded poly (ethylene imine) composite hydrogels with highly efficient catalytic reduction of 4-nitrophenol, ACS Omega 5 (7) (2020) 3725–3733.
[15] L. Zhang, J. Yin, K. Wei, B. Li, T. Jiao, Y. Chen, et al., Fabrication of hierarchical $SrTiO_3$@ MoS_2 heterostructure nanofibers as efficient and low-cost electrocatalysts for hydrogen-evolution reactions, Nanotechnology 31 (20) (2020) 205604.
[16] C.M. Vu, D.D. Nguyen, T.D. Pham, L.T. Pham, H.J. Choi, Environmentally benign green composites based on epoxy resin/bacterial cellulose reinforced glass fiber: fabrication and mechanical characteristics, Polym. Test. 61 (2017) 150–161.
[17] D.D. La, S.V. Bhosale, L.A. Jones, N. Revaprasadu, S.V. Bhosale, Fabrication of a Graphene@ TiO2@ Porphyrin hybrid material and its photocatalytic properties under simulated sunlight irradiation, ChemistrySelect 2 (11) (2017) 3329–3333.
[18] Z. Hua, J. Zhang, X. Bai, Z. Ye, Z. Tang, L. Liang, et al., Aggregation of TiO_2-graphene nanocomposites in aqueous environment: influence of environmental factors and UV irradiation, Sci. Total Environ. 539 (2016) 196–205.
[19] X. Fu, L.A. Clark, Q. Yang, M.A. Anderson, Enhanced photocatalytic performance of titania-based binary metal oxides: TiO2/SiO2 and TiO2/ZrO2, Environ. Sci. Technol. 30 (2) (1996) 647–653.
[20] Z. Liu, R.J. Davis, Investigation of the structure of microporous Ti-Si mixed oxides by X-ray, UV reflectance, FT-Raman, and FT-IR spectroscopies, J. Phys. Chem. 98 (4) (1994) 1253–1261.
[21] C.-D.-D. Dong, M.-L.-L. Tsai, C.-W.-W. Chen, C.-M.-M. Hung, Heterogeneous persulfate oxidation of BTEX and MTBE using Fe_3O_4-CB magnetite composites and the cytotoxicity of degradation products, In. Biodeter. Biodegr. 124 (2017) 109–118.
[22] A. Ghenaatgar, R. M.A.Tehrani, A. Khadir, Photocatalytic degradation and mineralization of dexamethasone using WO_3 and ZrO_2 nanoparticles: optimization of operational parameters and kinetic studies, J. Water Proc. Eng. 32 (2019) 100969.
[23] D. Hariharan, P. Thangamuniyandi, P. Selvakumar, U. Devan, A. Pugazhendhi, R. Vasantharaja, et al., Green approach synthesis of Pd@TiO_2 nanoparticles: characterization, visible light active picric acid degradation and anticancer activity, Proc. Biochem. 87 (2019) 83–88.
[24] D. Hariharan, P. Thangamuniyandi, A. Jegatha Christy, R. Vasantharaja, P. Selvakumar, S. Sagadevan, et al., Enhanced photocatalysis and anticancer activity of green hydrothermal synthesized Ag@TiO_2 nanoparticles, J. Photochem. Photobiol. B: Biol. 202 (2020) 111636.
[25] Y. Lin, S. Zhou, S.W. Sheehan, D. Wang, Nanonet-based hematite heteronanostructures for efficient solar water splitting, J. Am. Chem. Soc. 133 (8) (2011) 2398–2401.
[26] M.T. Mayer, C. Du, D. Wang, Hematite/Si nanowire dual-absorber system for photoelectrochemical water splitting at low applied potentials, J. Am. Chem. Soc. 134 (30) (2012) 12406–12409.
[27] K. Sivula, F. Le Formal, M. Grätzel, Solar water splitting: progress using hematite (α-Fe_2O_3) photoelectrodes, ChemSusChem 4 (4) (2011) 432–449.
[28] T.H. Jeon, W. Choi, H. Park, Photoelectrochemical and photocatalytic behaviors of hematite-decorated titania nanotube arrays: energy level mismatch versus surface specific reactivity, J. Phys. Chem. C 115 (14) (2011) 7134–7142.
[29] F. Meng, J. Li, S.K. Cushing, J. Bright, M. Zhi, J.D. Rowley, et al., Photocatalytic water oxidation by hematite/reduced graphene oxide composites, ACS Catal. 3 (4) (2013) 746–751.
[30] I. Thomann, B.A. Pinaud, Z. Chen, B.M. Clemens, T.F. Jaramillo, M.L. Brongersma, Plasmon enhanced solar-to-fuel energy conversion, Nano Lett. 11 (8) (2011) 3440–3446.
[31] Y. Katsuta, R. Akahane, K. Yahagi, Electrical properties of rutile (TiO_2) thin film, Jap. J. Appl. Phys. 10 (8) (1971) 976.
[32] H. Tang, K. Prasad, R. Sanjines, P. Schmid, F. Levy, Electrical and optical properties of TiO_2 anatase thin films, J. Appl. Phys. 75 (4) (1994) 2042–2047.
[33] W.-H.-H. Hung, T.-M.-M. Chien, C.-M.-M. Tseng, Enhanced photocatalytic water splitting by plasmonic TiO_2-Fe_2O_3 cocatalyst under visible light irradiation, J. Phys. Chem. C 118 (24) (2014) 12676–12681.
[34] E.S. Mora, E.G. Barojas, E.R. Rojas, R.S. González, Morphological, optical and photocatalytic properties of TiO_2-Fe_2O_3 multilayers, Sol. Energy Mater. Sol. Cells 91 (15–16)) (2007) 1412–1415.
[35] W.J. Chung, D.D. Nguyen, X.T. Bui, S.W. An, J.R. Banu, S.M. Lee, et al., A magnetically separable and recyclable Ag-supported magnetic TiO_2 composite catalyst: fabrication, characterization, and photocatalytic activity, J. Environ. Manage. 213 (2018) 541–548.
[36] N. You, X.-F.-F. Wang, J.-Y.-Y. Li, H.-T.-T. Fan, H. Shen, Q. Zhang, Synergistic removal of arsanilic acid using adsorption and magnetic separation technique based on Fe_3O_4@ graphene nanocomposite, J. Ind. Eng. Chem. 70 (2019) 346–354.
[37] Q.-U.-U. Ain, M.U. Farooq, M.I. Jalees, Application of magnetic graphene oxide for water purification: heavy metals removal and disinfection, J. Water Proc. Eng. 33 (2020) 101044.
[38] P.K. Surolia, R.J. Tayade, R.V. Jasra, Effect of anions on the photocatalytic activity of Fe (III) salts impregnated TiO_2, Ind. Eng. Chem. Res. 46 (19) (2007) 6196–6203.

[39] H. Su, X. Lv, Z. Zhang, J. Yu, T. Wang, Arsenic removal from water by photo-catalytic functional Fe_2O_3-TiO_2 porous ceramic, J. Porous Mater. 24 (5) (2017) 1227–1235.
[40] P.T. Nguyen, D.A. Nguyen, P.T. Nguyen, B.T. Le, P.T.H.T. Nguyen, D.D. La, Low-cost fabrication of Fe2O3/rutile nanocomposite from Ilmenite ore: a highly effective adsorbent for removal of arsenic in aqueous media, Adv. Nat. Sci. Nanosci. Nanotechnol. 10 (1) (2019) 015014.
[41] W. Phoohinkong, W. Yimwan, W. Mekprasart, W. Pecharapa, Preparation of nano $FeTiO_3$-TiO_2 catalyst from ilmenite ore for catalytic degradation of methylene blue, Suranaree J. Sci. Technol. 23 (4) (2016).
[42] Y.R. Smith, K.J.A. Raj, V.R. Subramanian, B. Viswanathan, Sulfated Fe_2O_3-TiO_2 synthesized from ilmenite ore: a visible light active photocatalyst, Coll. Surf. A Phys. Chem. Eng. Asp. 367 (1-3) (2010) 140–147.
[43] S. Anuradha, K. Raj, V. Vijayaraghavan, B. Viswanathan, Sulphated Fe_2O_3-TiO_2 catalysed transesterification of soybean oil to biodiesel, Indian J. Chem. 53A (2014) 1493–1499.
[44] L. Zhang, Z. Wang, X. Xu, C. Chen, B. Gao, X. Xiao, Insights into the phosphate adsorption behavior onto 3D self-assembled cellulose/graphene hybrid nanomaterials embedded with bimetallic hydroxides, Sci. Total Environ. 653 (2019) 897–907.
[45] R. Samiee, B. Ramezanzadeh, M. Mahdavian, E. Alibakhshi, G. Bahlakeh, Graphene oxide nano-sheets loading with praseodymium cations: adsorption-desorption study, quantum mechanics calculations and dual active-barrier effect for smart coatings fabrication, J. Ind. Eng. Chem. 78 (2019) 143–154.
[46] A.A. Javidparvar, R. Naderi, B. Ramezanzadeh, G. Bahlakeh, Graphene oxide as a pH-sensitive carrier for targeted delivery of eco-friendly corrosion inhibitors in chloride solution: experimental and theroretical investigations, J. Ind. Eng. Chem. 72 (2019) 196–213.
[47] E.J.S. Christy, S. Gopi, A. Rajeswari, G. Sudharsan, A. Pius, Highly crosslinked 3-D hydrogels based on graphene oxide for enhanced remediation of multi contaminant wastewater, J. Water Proc. Eng. 31 (2019) 100850.
[48] Y. Kopelevich, P. Esquinazi, Graphene physics in graphite, Adv. Mater. 19 (24) (2007) 4559–4563.
[49] S. Morozov, K. Novoselov, M. Katsnelson, F. Schedin, D. Elias, J. Jaszczak, et al., Giant intrinsic carrier mobilities in graphene and its bilayer, Phys. Rev. Lett. 100 (1) (2008) 016602.
[50] M.A. Ahsan, V. Jabbari, M.T. Islam, R.S. Turley, N. Dominguez, H. Kim, et al., Sustainable synthesis and remarkable adsorption capacity of MOF/graphene oxide and MOF/CNT based hybrid nanocomposites for the removal of Bisphenol A from water, Sci. Total Environ. 673 (2019) 306–317.
[51] L. De Marchi, C. Pretti, B. Gabriel, P.A.A.P. Marques, R. Freitas, V. Neto, An overview of graphene materials: properties, applications and toxicity on aquatic environments, Sci. Total Environ. 631–632 (2018) 1440–1456.
[52] L. Xu, Y. Yang, W. Li, Y. Tao, Z. Sui, S. Song, et al., Three-dimensional macroporous graphene-wrapped zero-valent copper nanoparticles as efficient micro-electrolysis-promoted Fenton-like catalysts for metronidazole removal, Sci. Total Environ. 658 (2019) 219–233.
[53] R. Beura, S. Rajendran, M.A. Gracia Pinilla, P. Thangadurai, Enhanced photo-induced catalytic activity of Cu ion doped ZnO - Graphene ternary nanocomposite for degrading organic dyes, J. Water Proc. Eng. 32 (2019) 100966.
[54] M. Ahmad, I. Bhatti, K. Qureshi, N. Ahmad, J. Nisar, M. Zuber, et al., Graphene oxide supported $Fe_2(MoO_4)_3$ nano rods assembled round-ball fabrication via hydrothermal route and photocatalytic degradation of nonsteroidal anti-inflammatory drug, J. Mol. Liq. 301 (2020) 112343.
[55] S. Ata, I. Shaheen, S. Ghafoor, M. Sultan, F. Majid, I. Bibi, et al., Graphene and silver decorated ZnO composite synthesis, characterization and photocatalytic activity evaluation, Diam. Relat. Mater. 90 (2018) 26–31.
[56] M. Mohsin, I.A. Bhatti, A. Ashar, A. Mahmood, Q. ul Hassan, M. Iqbal, Fe/ZnO@ ceramic fabrication for the enhanced photocatalytic performance under solar light irradiation for dye degradation, J. Mater. Res. Technol. (2020).
[57] Q. Xiang, J. Yu, M. Jaroniec, Graphene-based semiconductor photocatalysts, Chem. Soc. Rev. 41 (2) (2012) 782–796.
[58] Y. Chen, A. Li, Z.-H.-H. Huang, L.-N.-N. Wang, F. Kang, Porphyrin-based nanostructures for photocatalytic applications, Nanomaterials 6 (3) (2016) 51.
[59] W.-K.-K. Jo, Y. Won, I. Hwang, R.J. Tayade, Enhanced photocatalytic degradation of aqueous nitrobenzene using graphitic carbon-TiO_2 composites, Ind. Eng. Chem. Res. 53 (9) (2014) 3455–3461.
[60] Y. Chen, C. Zhang, X. Zhang, X. Ou, X. Zhang, One-step growth of organic single-crystal p-n nano-heterojunctions with enhanced visible-light photocatalytic activity, Chem. Commun. 49 (80) (2013) 9200–9202.
[61] C.H. Nguyen, R.-S.-S. Juang, Efficient removal of methylene blue dye by a hybrid adsorption-photocatalysis process using reduced graphene oxide/titanate nanotube composites for water reuse, J. Ind. Eng. Chem. 76 (2019) 296–309.
[62] D. Zhang, Y. Gao, X. Pu, W. Li, C. Su, P. Cai, et al., One-step combustion synthesis of magnetic Fe_2O_3/TiO2/graphene hybrids and their visible-light-driven photo-degradation of methylene blue, Sci. Adv. Mater. 6 (12) (2014) 2632–2639.
[63] M.D.D. La, S. Bhargava, S.V. Bhosale, Improved and a simple approach for mass production of graphene nanoplatelets material, ChemistrySelect 1 (5) (2016) 949–952.
[64] S.C. Lee, H.O. Lintang, L. Yuliati, High photocatalytic activity of Fe_2O_3/TiO_2 nanocomposites prepared by photodeposition for degradation of 2, 4-dichlorophenoxyacetic acid, Beilstein J. Nanotechnol. 8 (1) (2017) 915–926.
[65] D.D. La, R. Ramanathan, A. Rananaware, V. Bansal, S.V. Bhosale, Nanostructured charge transfer complex of CuTCNQF_4 for efficient photo-removal of hexavalent chromium, RSC Adv. 6 (40) (2016) 33931–33936.
[66] Y. Chen, Z.-H.-H. Huang, M. Yue, F. Kang, Integrating porphyrin nanoparticles into a 2D graphene matrix for free-standing nanohybrid films with enhanced visible-light photocatalytic activity, Nanoscale 6 (2) (2014) 978–985.
[67] D. Li, W. Dong, S. Sun, Z. Shi, S. Feng, Photocatalytic degradation of acid chrome blue K with porphyrin-sensitized TiO_2 under visible light, J. Phys. Chem. C 112 (38) (2008) 14878–14882.